Available online at www.sciencedirect.com
ScienceDirect
Journal of the European Ceramic Society 27 (2007) 3239–3251
www.elsevier.com/locate/jeurceramsoc

Microstructural characterization and crystallization kinetics of $(1-x)TeO_2$–xK_2O ($x = 0.05$, 0.10, 0.15, 0.20 mol) glasses

B. Öz [a], M.L. Öveçoğlu [a,*], I. Kabalcı [b], G. Özen [b]

[a] *Department of Metallurgical and Materials Engineering, Istanbul Technical University, Maslak, 34469 İstanbul, Turkey*
[b] *Department of Physics, Istanbul Technical University, 34469 İstanbul, Turkey*

Received 13 September 2006; received in revised form 27 December 2006; accepted 12 January 2007
Available online 29 March 2007

Abstract

Microstructural characterization and crystallization kinetics of $(1-x)TeO_2$–xK_2O ($x = 0.05$, 0.10, 0.15, and 0.20 in molar ratio) glasses were investigated using DTA, XRD, Raman spectroscopy, optical microscopy and SEM techniques. Whereas only one exothermic peak was observed for the $0.95TeO_2$–$0.05K_2O$ and $0.90TeO_2$–$0.10K_2O$ glasses, two crystallization peaks were present on the DTA plots of the $0.85TeO_2$–$0.15K_2O$ and $0.80TeO_2$–$0.20K_2O$ glasses. On the basis of the XRD and Raman spectrophometry investigations, α-TeO_2, γ-TeO_2 and $K_2Te_4O_9$ crystal phases were present in the $(1-x)TeO_2$–xK_2O ($x = 0.05$, 0.10, 0.15, and 0.20 in molar ratio) glass samples heated above the peak crystallization temperatures, T_p. SEM/EDS investigations of $(1-x)TeO_2$–xK_2O ($x = 0.05$, 0.10, 0.15, and 0.20 in molar ratio) glasses heated above T_p revealed the presence of distinct TeO_2-rich and $K_2Te_4O_9$ in the $0.95TeO_2$–$0.05K_2O$ and triangular wedge-shaped crystalline regions in the $0.90TeO_2$–$0.10K_2O$, $0.85TeO_2$–$0.15K_2O$ and $0.80TeO_2$–$0.20K_2O$ glasses. DTA analyses were carried out at different heating rates and the Avrami constant for the $0.95TeO_2$–$0.05K_2O$ glass was calculated as 0.94, an indication of surface crystallization also confirming SEM results. On the other hand, the n values were between 1.7 and 1.87 for the exothermic peaks of the $0.80TeO_2$–$0.10K_2O$, $0.85TeO_2$–$0.15K_2O$ and $0.80TeO_2$–$0.20K_2O$ glasses, indicating one-dimensional crystalline growth mechanisms for these glasses. Activation energies for one-dimensional crystal growth mechanisms in these crystals determined from the modified Kissinger plots were found to vary between 550 and 650 kJ/mol.

Keywords: TeO_2–K_2O glasses; Crystallization; Microstructure

1. Introduction

Among many oxide glasses, tellurite glasses have been investigated extensively due to their relative low-phonon energy, high refractive index,[1] high dielectric constant,[1,2] good corrosion resistance, thermal and chemical stability.[3,4] Owing to these physical properties, tellurite glasses are better than silicate, borate and phosphate glasses as potential candidates as the host materials for some infrared and infrared to visible upconversion applications in photonics such as optical data storage, lasers, sensors and optical displays.[5] Furthermore, they present large transparency from the near ultraviolet to the middle infrared region and are capable of incorporating large concentrations of rare-earth ions into the matrix and the large refractive index and the small phonon energy are desirable for radiative transitions of rare-earth ions.[1,3]

Due to anomalous glass-forming behaviour of tellurite glasses,[6] tellurium oxide (TeO_2) as the main but conditional glass former, does not transform to the glassy state as a pure oxide in normal conditions. The alkali oxide addition M_2O (where M = Li, Na, K, Rb or Cs) to TeO_2 based glasses increases their glass forming tendency and produces non-bridging oxygen (NBO) sites which decrease the average coordination number,[6,7] thus resulting in glasses that require only modest cooling over a specific range of added modifier and are resistant to crystallization.[6,8] An understanding of the crystallization behavior is important to develop and use TeO_2-based glasses as a laser material or an optical switching device, which will bear high thermal loads and thus will be subjected to crystallization during laser operation.[9] The investigation of crystallization kinetics in these glass systems has often been limited by the elaborate nature of the experimental procedures which are in

* Corresponding author. Tel.: +90 212 285 3355; fax: +90 212 285 3427.
E-mail address: ovecoglu@itu.edu.tr (M.L. Öveçoğlu).

0955-2219/$ – see front matter © 2007 Published by Elsevier Ltd.
doi:10.1016/j.jeurceramsoc.2007.01.010

use. The increasing use of thermoanalytical techniques, such as differential thermal analysis (DTA) or differential scanning calorimetry (DSC), has offered the promise of obtaining useful data with simple methods.[10] The relationship between glass structure and the added alkali metal ion concentration has been studied by means of Raman spectroscopy, high-temperature XRD, X-ray radial distribution function, and XAFS.[11,12] However, the nature and morphologies of crystalline structures based on the potassium–tellurite (TeO_2–K_2O) glasses has not yet been established.

The present study focuses on the crystallization kinetics and microstructural characterization of the TeO_2–K_2O glass system. Four different glass compositions, viz. the $0.95TeO_2$–$0.05K_2O$, $0.90TeO_2$–$0.10K_2O$, $0.85TeO_2$–$0.15K_2O$ and $0.80TeO_2$–0.20K2O glasses were investigated using DTA, X-ray diffractometry (XRD), Raman spectrophotometry, SEM and optical microscopy techniques. The crystalline phases corresponding to the exothermic transformations seen in the DTA scans, were identified by using the results of both Raman spectrophotometry and the X-ray diffractometry investigations. The DTA scans were used to determine the crystallization mechanisms and activation energy for the crystallization processes using the non-isothermal method. SEM and optical microscopy techniques were used to support the information obtained about the formation and size of the crystallizing phases detected in the DTA, XRD and Raman scans.

2. Experimental procedure

2.1. Glass synthesis

Four different glass samples of the binary system TeO_2–K_2O were prepared to constitute different chemical compositions of $(1-x)TeO_2$–xK_2O where $x = 0.05$, 0.10, 0.15 and 0.20 in molar ratio (now hereafter referred to as the $0.95TeO_2$–$0.05K_2O$, $0.90TeO_2$–$0.10K_2O$, $0.85TeO_2$–$0.15K_2O$ and $0.80TeO_2$–$0.20K_2O$ glasses, respectively). The starting materials were TeO_2 (99.995% purity, Chempur Co.) and K_2CO_3 (reagent-grade, 99.995% purity, Chempur Co.) powders. After preparing and thoroughly mixing powder batches weighing 7 g for each composition, melting was carried out using a platinum crucible with a closed lid in an electrically heated furnace at 900–950 °C for about 30 min, until CO_2 evolution ceased. The molten glass was removed from the furnace at 950 °C and was cast onto a graphite crucible which was immersed in a shallow water bath. To achieve homogeneity, the cast was crushed, pulverized and remelted at the same temperature for additional 30 min and was cast using the same procedure. Wet chemistry analyses carried out on bulk as-quenched and heat-treated TeO_2–K_2O glass samples revealed that the initial elemental stoichiometry of the bulk glass samples did not change after quenching and heat-treatment.

2.2. Thermal behavior and crystallization

Differential thermal analysis (DTA) scans of as-cast $0.95TeO_2$–$0.05K_2O$, $0.90TeO_2$–$0.10K_2O$, $0.85TeO_2$–$0.15K_2O$ and $0.80TeO_2$–$0.20K_2O$ glass specimens were carried out in Thermoflex Rigaku Thermal Analyzer equipped with PTC-10A Temperature Controller Unit to determine the characteristics glass transition temperatures (T_g), crystallization peak temperatures (T_p), and the melting temperatures (T_m). The glass powder, 50 mg, were heated at the rate of 10 °C/min from room temperature to 700 °C in a platinum crucible and using the same amount of alumina powder as the reference material. The crucibles used were matched pairs made of platinum and the temperature precision was ±1 °C. For the DTA curve of each as-cast glass, the T_g temperature is selected as the inflection point of the step change of the calorimetric signal[13] and the T_p temperature(s) is/are measured at the peak of crystallization. The effects of different heating rates on the crystallization peak temperatures (T_p) were examined through the DTA curves with the heating rates of 5, 10, 15 and 20 °C/min, to study the crystallization behavior of the glasses. The heat-treated glass samples were prepared by heating the as-cast glasses 15–20 °C above the crystallization peak temperatures obtained by DTA analyses, for 30 min, followed by quenching in air.

2.3. Microstructural characterization

The microstructural characterization of the as-cast and heat-treated glass samples were carried out using optical microscopy, electron microscopy, X-ray diffraction and Raman spectroscopy techniques. Optical microscopy (OM) investigations were performed in a Nikon™ Eclipse L150 microscope equipped with Nikon™ Coolpix 4.0 MP digital camera. Scanning electron microscopy (SEM) investigations were carried out both in a JEOL™ Model JSM 5410 operated at 15 kV and linked with Noran 2100 Freedom energy dispersive spectrometer (EDS) attachment and in a JEOL™ Model JSM-T330 operated at 25 kV and linked with a Zmax 30 Boron-up light element EDS detector. For the OM and SEM investigations, optical mount specimens were prepared using standard metallographical techniques followed by chemical etching in a 95% distilled water +5% HF solution for 20–30 s. The etched optical samples were coated with palladium–gold for the SEM and SEM/EDS study. X-ray diffraction (XRD) investigations were carried out in a Philips™ model PW3710 (Cu Kα radiation) diffractometer at 40 kV and 40 mV setting in the 2θ range from 10 to 90°. The crystallized phases were identified by comparing the peak positions and intensities with those in the JCPDS (Joint Committee on Powder Diffraction Standards) data files. The Raman spectra of the as-cast and crystallized samples were recorded on a FT Raman spectrophotometer (Digilab FTS 7000 Series) within the range of 0–1200 cm^{-1}. The digital intensity data was recorded at intervals of 1 cm^{-1}. A Nd:YAG laser system operating at 1064 nm was used as the excitation source and the specimen was excited with a power level of about 500 mW. The scattered radiation was detected by cooling Ge detector with a spectral resolution of 8 cm^{-1}.

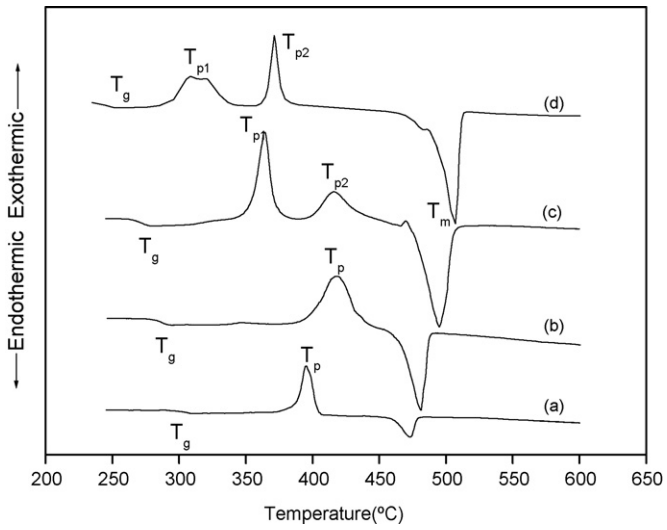

Fig. 1. DTA curves of as-cast samples of (a) $0.95TeO_2$–$0.05K_2O$ glass, (b) $0.90TeO_2$–$0.10K_2O$ glass, (c) $0.85TeO_2$–$0.15K_2O$ glass and (d) $0.80TeO_2$–$0.20K_2O$ glass, scanned at a rate of 10 °C/min.

3. Results and discussion

3.1. DTA investigations

Differential thermal analysis (DTA) investigations were conducted on the as-cast TeO_2–K_2O glasses. Fig. 1a–d illustrates the respective DTA thermograms of the as-cast $0.95TeO_2$–$0.05K_2O$, $0.90TeO_2$–$0.10K_2O$, $0.85TeO_2$–$0.15\ K_2O$ and $0.80TeO_2$–$0.20K_2O$ glass samples, all scanned at the heating rate of 10 °C/min. The glass transition (T_g), the peak crystallization temperatures (T_{p1} and T_{p2}) and melting temperature (T_m) are marked on the thermograms. As seen in Fig. 1, each DTA scan exhibits a small endothermic peak corresponding to the glass transition temperature, T_g. The T_g values, listed in Table 1, shift to lower values as the K_2O content increases. As seen in Fig. 1, the peak crystallization temperatures (T_p) occurred at a range of 327–421 °C following the glass transition temperatures for all four compositions. Whereas only one exotherm was observed for the $0.95TeO_2$–$0.05K_2O$ (Fig. 1a) and $0.90TeO_2$–$0.10K_2O$ glasses (Fig. 1b), two exotherms are present for the $0.85TeO_2$–$0.15K_2O$ (Fig. 1c) and $0.80TeO_2$–$0.20K_2O$ glasses (Fig. 1d). All exothermic peaks of Fig. 1 can be ascribed to the formation and/or transformation of crystalline phases.

Table 1
Values of glass transition, T_g, crystallization, T_{p1} and T_{p2}, and melting, T_m, temperatures of the $(1-x)TeO_2$–xK_2O glasses

K_2O content (mol%)	T_g (°C)	T_{p1} (°C)	T_{p2} (°C)	T_m (°C)
5	310	394	–	472
10	297	421	–	481
15	275	364	418	485
20	251	327	371	507

3.2. XRD results

On the basis of DTA results, X-ray diffractometry scans were carried out to verify the nature of crystallizing phases in the glassy matrix at temperatures above T_g for all glasses of the present investigation. Fig. 2a shows the X-ray diffraction patterns of the $(1-x)TeO_2$–xK_2O glasses ($x = 0.05$, 0.10, 0.15, 0.20) in the as-cast condition. As seen from Fig. 2a, the XRD patterns of all glass samples exhibit a large amount of peak broadening at 2θ values ranging between 26 and 29° which indicates typical amorphous clustering of glassy solids. Further, whereas no crystalline peaks were detected for the $0.95TeO_2$–$0.05K_2O$ glass in the as-cast condition, XRD peaks around $2\theta = 45°$ existed for the $0.90TeO_2$–$0.10K_2O$, $0.85TeO_2$–$0.15K_2O$ and $0.80TeO_2$–$0.20K_2O$ glasses in the as-cast condition. The Bragg angle of $\theta = 22.5°$ for the Cu Kα radiation conditions ($\lambda = 0.15418$ nm) corresponds unambiguously to the highest intensity peak of the $K_2Te_4O_9$ phase which

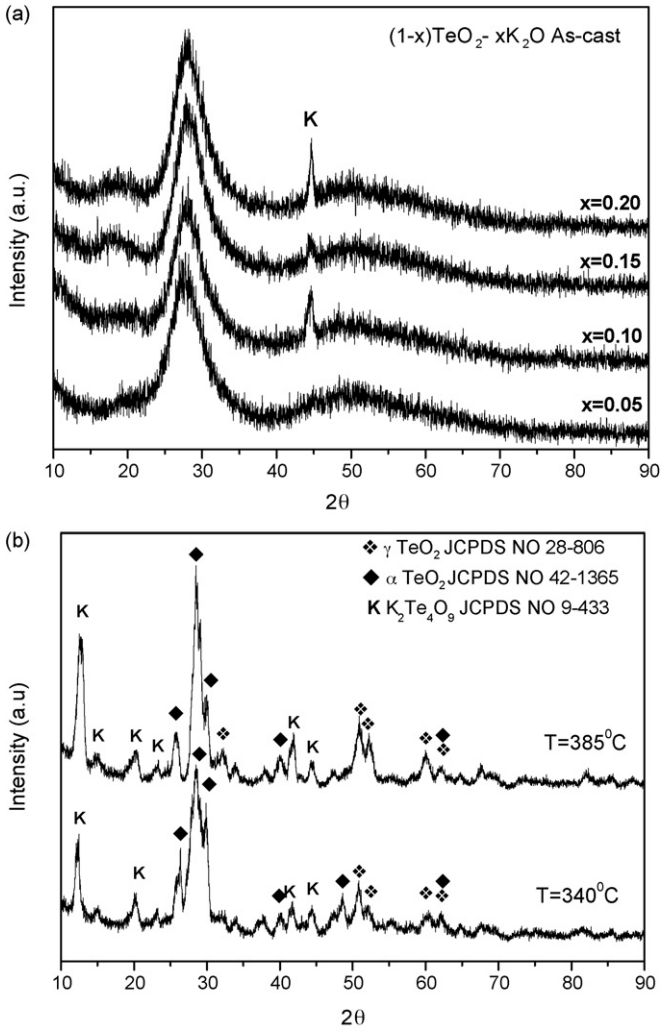

Fig. 2. X-ray diffraction patterns taken from (a) $(1-x)TeO_2$–xK_2O glasses ($x = 0.05$, 0.10, 0.15, 0.20) in the as-cast condition, and from the (b) $0.80TeO_2$–$0.20K_2O$ glass heated to 340 and 385 °C, all heated at a rate of 10 °C/min, held for 30 min. at these temperatures followed by quenching in air.

has a centrosymmetric monoclinic space group $P2_1/c$ but is regarded as a tetragonal Bravais lattice,[14] with lattice parameters of $a = 0.757$ nm, $b = 0.773$ nm and $c = 1.782$ nm.[14,15] Hart[14] and Tagg[16] also reported that the formation of the $K_2Te_4O_9$ ceramic phase, which arises as a result of bimodal phase separation in tellurium-based glasses with K_2O addition varying between 5 and 30 mol% K_2O content.

The XRD patterns of the $0.95TeO_2$–$0.05K_2O$, $0.90TeO_2$–$0.10K_2O$ and $0.85TeO_2$–$0.15K_2O$ glasses heated above their peak crystallization temperatures (T_p) followed by quenching in air were reported recently by the present authors[17] in a parallel study of the ongoing investigation. It was found that the XRD patterns of these glasses in the heat-treated conditions (heated above peak crystallization temperatures) matched the JCPDS card values of the paratellurite (α-TeO_2) phase which has a tetragonal crystal structure with lattice parameters $a = 0.481$ nm and $c = 0.761$ nm,[18] the new polymorph γ-TeO_2[19] phase named by Blanchandin et al.[20] having the orthorhombic symmetry with the calculated lattice parameters $a = 0.845$ nm, $b = 0.499$ nm and $c = 0.430$ nm and the $K_2Te_4O_9$ phase also identified in the as-cast $0.90TeO_2$–$0.10K_2O$, $0.85TeO_2$–$0.15K_2O$ and $0.80TeO_2$–$0.20K_2O$ glasses(Fig. 2a). The XRD patterns of the $0.80TeO_2$–$0.20K_2O$ glass heated to 340 and 385 °C (above the peak crystallization temperatures) at a rate of 10 °C/min followed by quenching in air are given in Fig. 2b. All peaks of Fig. 2b are identified to belong to the stable α-TeO_2, metastable γ-TeO_2 and the $K_2Te_4O_9$ phases. In other words, the crystallization peaks shown in the DTA scans for the $0.80TeO_2$–$0.20K_2O$ (Fig. 1d) glass samples are the result of the simultaneous crystallization of both polymorphs of TeO_2: the stable α-TeO_2 phase and the metastable γ-TeO_2 phase. Thus, similar to the $0.95TeO_2$–$0.05K_2O$, $0.90TeO_2$–$0.10K_2O$ and $0.85TeO_2$–$0.15K_2O$ glasses,[17] the XRD pattern of the $0.80TeO_2$–$0.20K_2O$ glass sample heat-treated above the first and second exothermic transformations revealed the co-existence of α-TeO_2, γ-TeO_2 and $K_2Te_4O_9$ phases. On the basis of our previous work[17] and Fig. 2b, we believe that the second exotherm in the DTA curves of the $0.85TeO_2$–$0.15K_2O$ and the $0.80TeO_2$–$0.20K_2O$ glass samples (Fig. 1c and d) correspond to γ-$TeO_2 \rightarrow \alpha$-TeO_2 transformation, also reported previously for the $0.85TeO_2$–$0.15WO_3$ glasses.[20,21]

3.3. Raman spectra

Fig. 3a illustrates the Raman spectra of $(1-x)TeO_2$–xK_2O glasses in the as-cast condition, obtained at room temperature. In general, these spectra are composed of three main spectral regions: low-frequency region (50–200 cm^{-1}), intermediate region (200–550 cm^{-1}) and high-frequency region (550–900 cm^{-1}).[22,23] In the low-frequency region, there is an asymmetric Raman band ranging from 110 to 195 cm^{-1}, which shows a strong peak at about 167.5 cm^{-1}. This peak is attributed to the vibration of the Boson peak,[24,25] which is universal in the Raman spectra of non-crystalline solids, such as glasses.[24] Two Raman bands at around 265 and 460 cm^{-1} are seen in the intermediate region. The peak at about 460 cm^{-1} is attributed to the bending and stretching vibrations of the Te–O–Te or O–Te–O linkages.[11,12] In the high-frequency region, the Raman spectra had two Raman bands at around 670 and 770 cm^{-1}. These bands are ascribed to the stretching mode of the TeO_3 trigonal pyramid (tp) units containing terminal Te–O bonds such as Te=O and Te–O^- with non-bridging oxygen atoms (NBO), the stretching mode of TeO_4 trigonal bipyramid (tbp) units with bridging oxygen atoms (BO) and the bending mode of Te–O–Te or O–Te–O linkages, respectively.[11,12,26] The amplitude of the 770 cm^{-1} band becomes larger, and the amplitudes of the 670 cm^{-1} band become smaller as the K_2O content increases. This result shows that the addition of K_2O, brings about the conversion of the TeO_4 tbp units with BO into the TeO_3 tp units with NBO in the TeO_2–K_2O samples.[12,26] Table 2 is a summary list of Raman band assignments for the $(1-x)TeO_2$–$(x)K_2O$ glasses.[11,22–25,29]

The Raman shift peaks of the Raman scans for all the glass samples heated above their respective peak crystallization temperatures, at a rate of 10 °C/min followed by quenching in air, were identified according to the Raman spectroscopy information of the TeO_2 based glasses reported by Sekiya et al.,[11] Mirgorodsky et al.[27] and Chowdari et al.[28] The Raman spectra of α-, β- and γ-TeO_2 crystalline phases present in TeO_2-based glasses has been reported by Mirgorodsky.[27] Fig. 3b and c are the respective Raman spectra of $0.95TeO_2$–$0.05K_2O$ and $0.90TeO_2$–$0.10K_2O$ glasses heated above peak crystallization temperatures of 425 °C and 440 °C, respectively. Both spectra are almost identical with each other and pertain to both the stable α-TeO_2 and metastable α-TeO_2 phases. The exact assignment of the Raman peaks can be made by consulting the relevant literature: i.e. α-TeO_2[27,28] as having the spectral peaks at about 400, 600 and 650 cm^{-1} and γ-TeO_2[29] having the spectral peaks at about 720 and 760 cm^{-1}. According to Akagi et al.,[12] the peak having a Raman value of 720 cm^{-1} shows that large proportion of the crystals consist of TeO_3 tp units which remained from uncrystallized conditions of glass. Charton et al.[29] assigned the peak at 660 cm^{-1} to TeO_4 trigonal bipyramids encountered in the stable α-TeO_2 and attributed the shoulder centered at 760 cm^{-1} to the metastable γ-TeO_2 phase which they expressed that this phase can only appear as a shoulder in the vicinity of Raman peaks of the stable α-TeO_2 phase. Further, Charton et al.[29] expressed that the band around 450 cm^{-1} is due to the presence of at least two kinds of Te–O–Te bridging bonds. On the basis of these relevant literature and assuming that the spectral peaks between 0 and 200 cm^{-1} are the Boson peaks, there remains three unidentified peaks for the crystallized $0.95TeO_2$–$0.05K_2O$ and $0.90TeO_2$–$0.10K_2O$ glasses: at 226, 285 and 331 cm^{-1}. Based on the XRD results of these glasses in the heat-treated condition,[17] we believe that these

Table 2
Raman band assignments for the $(1-x)TeO_2$–xK_2O glasses[11,22–25,29]

Wave number (cm^{-1})	Vibration mode
460–485	Stretching vibrations of Boson bands
650–680	Bending and stretching vibrations of Te–O–Te or O–Te–O linkages Stretching vibrations of TeO_4 tbp
725–745	Stretching vibrations of TeO_3 tp

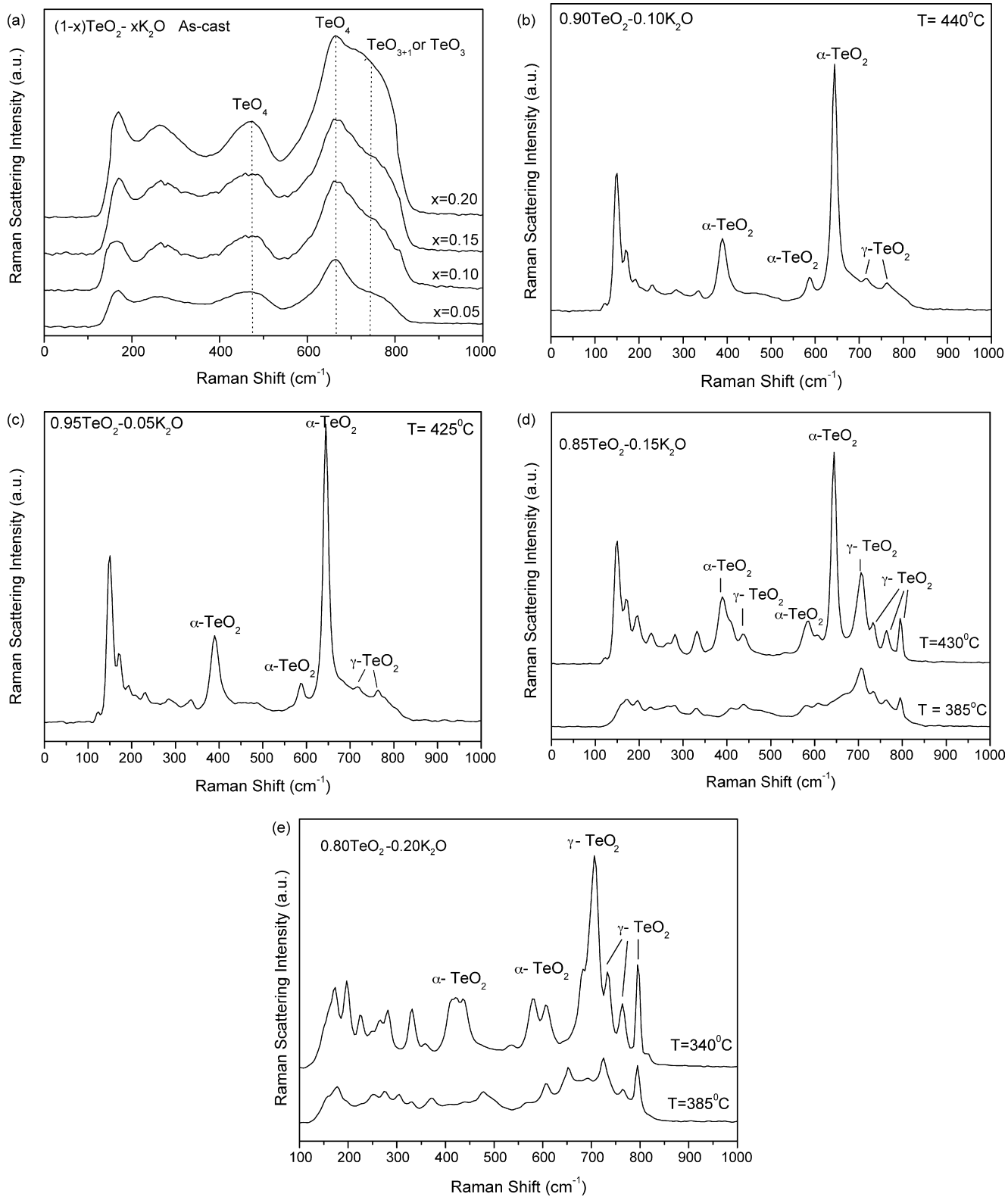

Fig. 3. Raman spectra taken from (a) $(1-x)TeO_2$–xK_2O glasses ($x = 0.05, 0.10, 0.15, 0.20$) in the as-cast condition, and from (b) 0.95 TeO_2–$0.05K_2O$ glass heated to 425 °C, (c) $0.90TeO_2$–$0.10K_2O$ glass heated to 440 °C, (d) $0.85TeO_2$–$0.15K_2O$ glass heated to 385 °C and 430 °C, (e) $0.80TeO_2$–$0.20K_2O$ glass heated to 340 and 385 °C. All heated at a rate of 10 °C/min, held for 30 min at these temperatures followed by quenching in air.

three unidentified spectral peaks might belong to the K_2Te4O_9 phase.

In the case of $0.85TeO_2$–$0.15K_2O$ samples heated above the crystallization temperatures, Raman spectra of the $85TeO_2$–$0.15K_2O$ glass heated to $T = 385\,^{\circ}C$ (the first crystallization temperature), shown in Fig. 3d, indicates the fact that most of the identifiable spectral peaks belong to the γ-TeO_2 phase except 2 minute ones at 407 and 600 cm^{-1} which are believed to be pertaining to the α-TeO_2 phase. On the other hand, Raman spectra of the same glass heated to $T = 430\,^{\circ}C$ (the second crystallization temperature), shown in Fig. 3d, is a result of two tellurite polymorphs (transformed α-TeO_2 and retained γ-TeO_2). Similar to Fig. 3b and c, the range between 0 and 200 cm^{-1} in Fig. 3d is disregarded as the Boson range and the spectral peaks at 226, 285 and 331 cm^{-1} are believed to belong to the $K_2Te_4O_9$ phase. In addition, the peak at 585 cm^{-1} can be ascribed to terminal Te–O bonds, thus belongs to the α-TeO_2 stable phase.[27]

Fig. 3e presents the Raman spectra of the $0.80TeO_2$–$0.20K_2O$ glass heated to $T = 340\,^{\circ}C$ (first crystallization peak temperature) and to $T = 385\,^{\circ}C$ (second crystallization peak temperature), respectively. Similar to that of the 0.85TeO2–$0.15K_2O$ glass (Fig. 3d), Fig. 3e also revealed the existence of the γ-TeO_2 and α-TeO_2 phases for both crystallization temperatures and the unidentified peaks at 226, 285 and 331 cm^{-1} may be due to $K_2Te_4O_9$ phase. There are noteworthy differences between the spectra of both glasses after the first and second crystallization temperatures. For both glasses, the shallow nature of spectral peaks after the first crystallization temperature as opposed to sharper counterparts after second crystallization temperature is an indication of the presence of larger quantities of uncrystallized parent glass phase after the first crystallization temperatures.

3.4. SEM and SEM/EDS investigations

SEM and SEM/EDS investigations were performed on the crystallized $(1-x)TeO_2$–xK_2O glasses of the present investigation in order to identify and analyze the morphology, size and chemistry of the crystallizing phases. For all samples, surface and cross-section SEM micrographs were taken in the secondary electron imaging (SEI) mode. Fig. 4a and b are a series of surface SEM/SEI micrographs and Fig. 4c is that taken at a tilt angle of 55° showing both the surface and the cross-section of the $0.95TeO_2$–$0.05K_2O$ glass sample heated to 425 °C followed by air-quenching. Fig. 4a is a representative SEM/SEI micrograph which reveals the presence of long (elongated) centrosymmetric stripe-shaped crystals varying between 20 and 30 μm in width and about 120 and 220 μm in length. EDS spectra taken from these elongated crystalline regions (labeled by *T* in Fig. 4a) revealed that they contained 80.6 ± 0.5 wt.% Te, 0.5 ± 0.02 wt.% K and 18.8 ± 0.4 wt.% O, which confirms

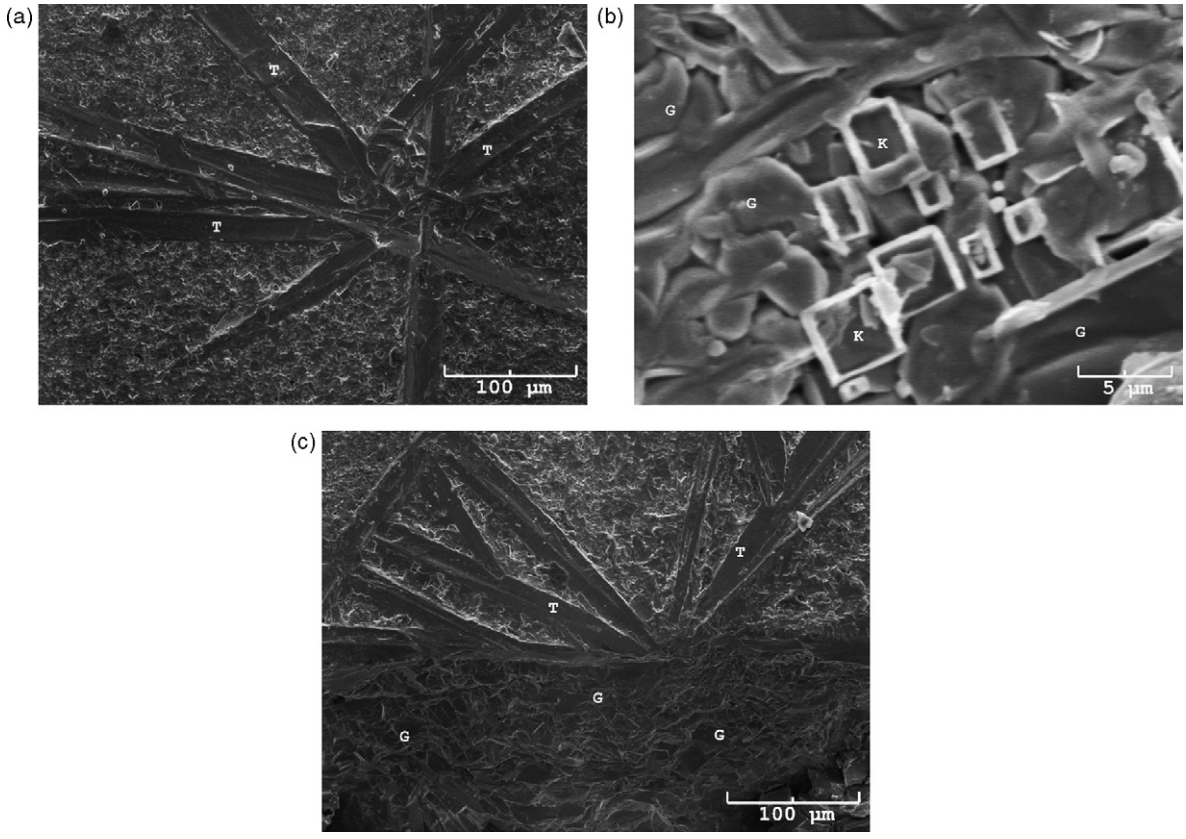

Fig. 4. (a and b) Typical SEM micrographs at various magnifications taken from the surface regions of the $0.95TeO_2$–$0.05K_2O$ sample heated to 425 °C at a rate of 10 °C/min, held for 30 min at this temperature followed by quenching in air. (c) A SEM micrograph taken from the same sample at a tilt angle of 55° showing both the surface and the cross-section.

that these crystalline regions are TeO_2-rich regions (i. e. containing α-TeO_2 and/or γ-TeO_2 phases). Fig. 4b is a SEM/SEI micrograph taken from a different location on the surface of the $0.95TeO_2$–$0.05K_2O$ glass sample revealing square- and/or rectangle-shaped grains varying between 2 and 5 μm in size surrounded by nodular/angular-shaped grains. EDS spectra taken from the rectangular/square-shaped grains (labeled by K in Fig. 4b) revealed that these grains contained 68.2 ± 0.8 wt.% Te, 10.9 ± 0.4 wt.% K and 21.0 ± 0.5 wt.% O, indicating the fact they belong to the $K_2Te_4O_9$ crystalline phase also detected in the XRD scan (Fig. 2b). In addition, EDS spectra taken from the surrounding regions G in Fig. 4b and c revealed the elemental chemistry of 91.3 ± 1.3 wt.% Te, 1.7 ± 0.2 wt.% K and 6.3 ± 0.6 wt.% O. In other words, the chemistry of these regions (regions G) are different from those of the previous ones (regions T and K) and considering the EDS stoichiometry, they are the amorphous glass matrix. Fig. 4c is a cross-sectional SEM micrograph taken at a tilt angle of about 55° from the $0.95TeO_2$–$0.05K_2O$ glass sample heated to 425 °C followed by air-quenching. It is evident from Fig. 4c that TeO_2-rich surface crystal stripes emanate from the edge of the sample and that there are no crystalline regions in the cross-section as revealed by the overall EDS analyses (taken from regions G). Thus, on the basis of Fig. 4c, it can be inferred that surface crystallization is the predominant mechanism for the $0.95TeO_2$–$0.05K_2O$ glass sample.

Fig. 5a and b present the SEM/SEI micrographs of the $0.90TeO_2$–$0.10K_2O$ sample heated to 440 °C, taken from the surface and the cross-section, respectively. Fig. 5a shows triangular wedge-shaped regions in various orientations. EDS analyses taken from different locations on these regions (regions KT in Fig. 5a) show that these regions contain 74.2 ± 0.3 wt.% Te, 6.5 ± 0.4 wt.% K and 18.2 ± 0.3 wt.% O, indicating that these consist of the TeO_2 and $K_2Te_4O_9$ phases in various amounts. Surrounding these regions is the amorphous glass matrix as indicated by the EDS spectra taken from three different locations (regions G in Fig. 5a). Fig. 5b is a cross-sectional SEM/SEI micrograph which shows long crystalline regions (regions KT) having a similar EDS chemistry to that of the surface which are surrounded by amorphous glassy regions (regions G).

Fig. 6a and b shows the respective SEM micrographs taken from the surface and the cross-section of $0.85TeO_2$–$0.15K_2O$ glass, heated to 385 °C (first exotherm in Fig. 1c) followed by quenching in air. As seen in Fig. 6a and 6b, both surface and cross-sectional microstructures have similar morphological features and both resemble the surface micrograph of the $0.90TeO_2$–$0.10K_2O$ sample heat-treated to 440 °C (Fig. 5a). Detailed EDS analyses from different regions revealed the presence of a combination of the TeO_2 and $K_2Te_4O_9$ phases in the crystalline regions (regions KT in Fig. 6a and b) and the amorphous glass matrix (regions G in Fig. 6a and b), inferring a microstructural chemistry similar to the $0.90TeO_2$–$0.10K_2O$ sample heat-treated to 440 °C (Fig. 5a) and verifying the nature of the phases in Fig. 2d. The SEM micrographs taken from the surface and the cross-section of the $0.85TeO_2$–$0.15K_2O$ sample heat-treated at 430 °C are given in Fig. 6c and d. The micrographs show rectangular-shaped crystals stacked in 2D-orientation with the crystal sizes ranging between 5–10 μm in width and 5–15 μm in length. EDS spectra taken from the crystalline regions (regions K in Fig. 6c and d) show that these regions had the chemical stoichiometry of 67.7 ± 0.5 wt.% Te, 11.2 ± 0.5 wt.% K and 21.3 ± 0.4 wt.% O. This indicates the existence of $K_2Te_4O_9$-rich crystals surrounded by a glassy matrix (regions G) both on the surface and in the cross-section.

Fig. 7a and b show the respective SEM micrographs taken from the surface and the cross-section of the $0.80TeO_2$–$0.20K_2O$ sample heat-treated to 340 °C (first exotherm in Fig. 1d) followed by quenching in air. Fig. 7a is a representative SEM/SEI micrograph which reveals the presence of large centrosymmetric crystals emanating from a center as long plates. EDS spectra taken from these plates (regions KT in Fig. 7a) show that these regions had a mean composition values of 73.4 ± 1.1 wt.% Te, 7.8 ± 0.5 wt.% K and 19.6 ± 0.4 wt.% O, indicating the existence of TeO_2 and $K_2Te_4O_9$ phases. SEM micrograph (Fig. 7b) taken from the cross section of the $0.80TeO_2$–$0.20K_2O$ sample heat-treated to 340 °C shows the morphology of a brittle fracture with cleavage surfaces. EDS spectra taken from several locations (regions G in Fig. 7b) of the cross-section revealed a mean chemical composition value close to the nominal composition, indicating the presence of only the amorphous glass matrix in the

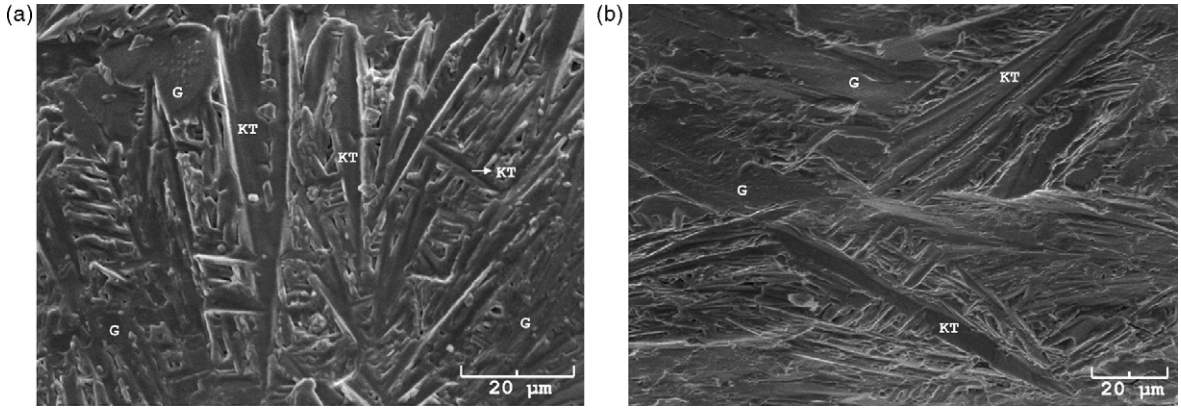

Fig. 5. Typical SEM micrographs taken from (a) surface region and (b) cross-section of the $0.90TeO_2$–$0.10\ K_2O$ sample heated to 440 °C at a rate of 10 °C/min and held for 30 min at this temperature followed by quenching in air.

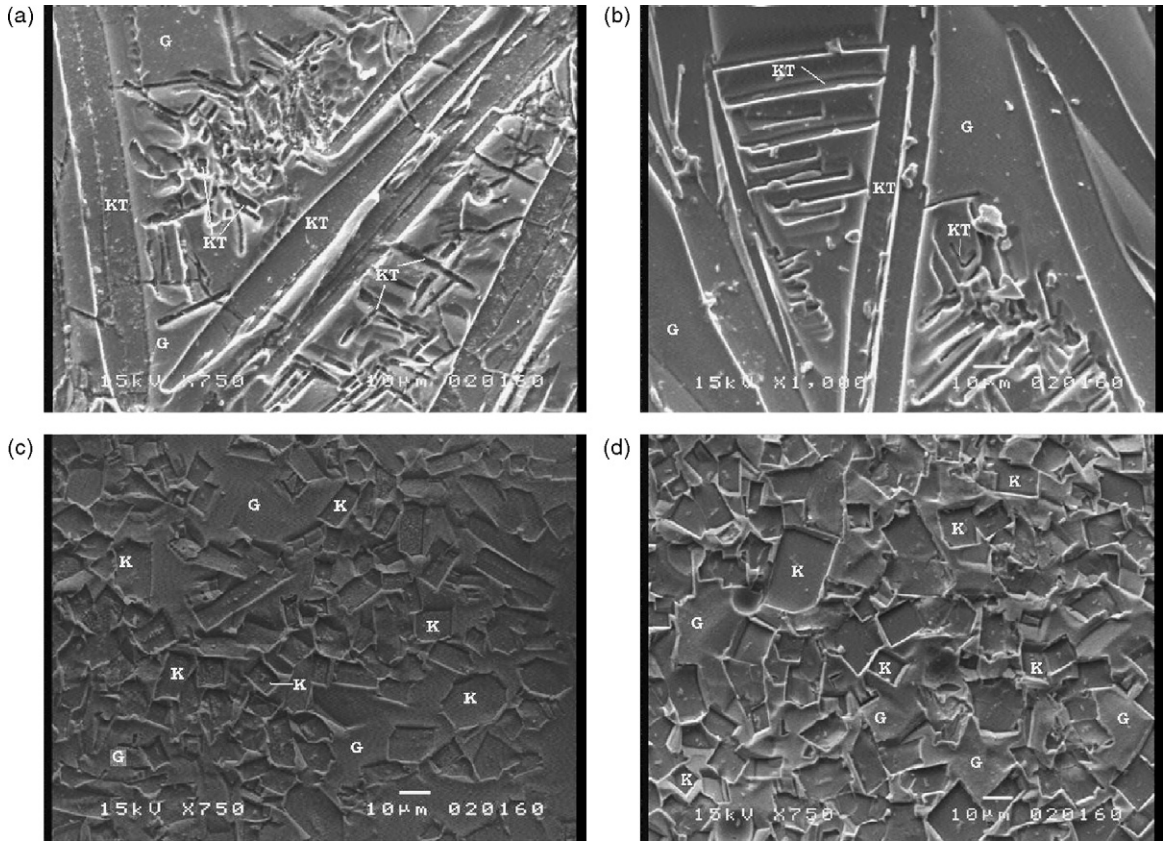

Fig. 6. Typical SEM micrographs taken from (a) surface region, (b) cross-section of the $0.85TeO_2$–$0.15K_2O$ glass heated to 385 °C and (c) surface region and (d) cross-section of the same sample heated to 430 °C. Both samples were heated at a rate of 10 °C/min., held for 30 min. at these temperatures followed by quenching in air.

bulk of this sample. Thus, on the basis of SEM/EDS investigations, only surface crystals are present in the $0.80TeO_2$–$0.20K_2O$ sample heat-treated to 340 °C followed by quenching in air. Fig. 7c and d are the representative SEM micrographs taken from the surface and the cross-section of the $0.80TeO_2$–$0.20K_2O$ sample heated to 385 °C (second exotherm in Fig. 1d), respectively. Crystalline plates between 10–25 μm in length and 5–7 μm in thickness stacked in random orientation are present on the surface of the $0.80TeO_2$–$0.20K_2O$ sample (Fig. 7c). EDS analyses taken from these crystals (regions K in Fig. 7c) revealed that they contained 71.5 ± 1.0 wt.% Te, 9.2 ± 0.4 wt.% K and 18.9 ± 0.3 wt.% O, suggesting that they have $K_2Te_4O_9$ and TeO_2 phases in various amounts. Fig. 7d is a SEM micrograph taken from the cross section of the $0.80TeO_2$–$0.20K_2O$ sample heat-treated to 385 °C (second exotherm in Fig. 1d) which reveals crystalline phases (regions K in Fig. 7d) and amorphous, glassy regions (regions K in Fig. 7d) in the microstructure.

3.5. Activation energy determination

Fig. 8a and b illustrate the DTA thermograms of the as-cast $0.95TeO_2$–$0.05K_2O$, $0.90TeO_2$–$0.10K_2O$, $0.85TeO_2$–$0.15\ K_2O$ and $0.80TeO_2$–$0.20\ K_2O$ glass samples scanned at the heating rates of 5, 10, 15 and 20 °C/min, respectively. For all exothermic peaks of Fig. 8a–c and for the second exothermic peak of Fig. 8d, the faster the heating rates, the higher the peak temperatures and larger the peak heights become. The T_g and T_p temperatures shift to higher values with increasing rate, a behavior also reported in the thermal studies of other glass systems.[21,30,31] However, completely paradoxical to this behaviour are the first exothermic peaks of the $0.80TeO_2$–$0.20\ K_2O$ glass sample (Fig. 8d) whose first exothermic peak of the DTA thermograms scanned at 15 and 20 °C/min lagged behind that scanned at 10 °C/min. The reason to this anomaly is not known.

The shift of peak temperatures with different heating rates in a non-isothermal DTA study was first analyzed by Kissinger[32] in the study of kinetics of chemical reactions. Later, his method was used by Matusita et al.[33] to study the crystallization peaks observed above the glass transition temperatures.[33,34] As shown by Matusita and Sakka,[34] if the number of crystal nuclei formed at temperature above T_g can be assumed to be constant in a glass matrix, then the rate of change of volume fraction of crystals can be defined as

$$\ln\left(\frac{\Phi^n}{T_p^2}\right) = -\frac{mQ}{RT_p} + \text{constant} \quad (1)$$

where Φ is the heating rate, T_p the peak crystallization temperature for a given Φ, Q the activation energy for crystallization, R the gas constant ($R = 8.31$ J/K mol), n the Avrami parameter and

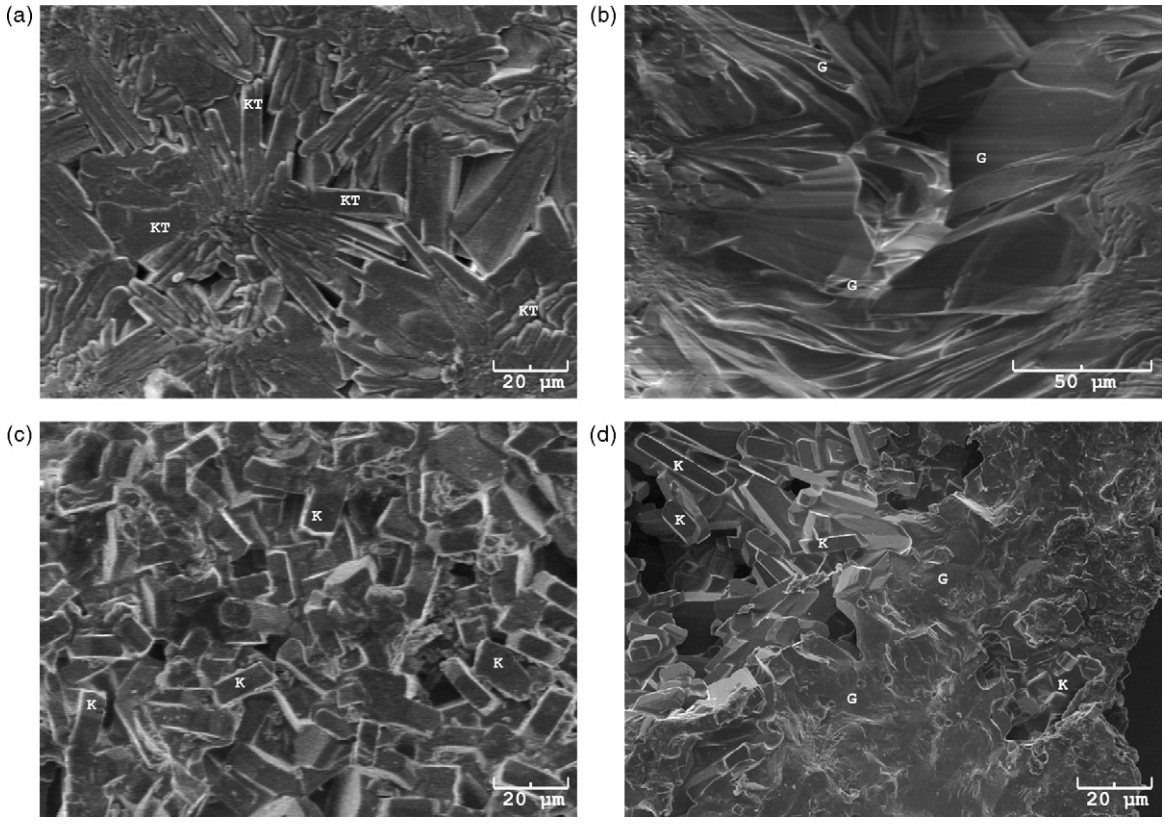

Fig. 7. Typical SEM micrographs taken from (a) surface region, (b) cross-section of the $0.80TeO_2$–$0.20K_2O$ glass heated to 340 °C and (c) surface region and (d) cross-section of the same glass heated to 385 °C Both samples were heated at a rate of 10 °C/min, held for 30 min at declared temperatures followed by quenching in air.

m is the dimensionality of crystal growth. Both n and m are characteristics of various crystallization mechanisms. As given in Table 3, depending on the governing crystallization mechanism, the parameters n and m can have various values; $m = 1$ when the predominant mechanism is surface crystallization and $m = 3$ for bulk crystallization.[33,34] For a non-isothermal DTA study, the nucleation takes place during DTA and $m = n - 1$. However, for the special case where surface crystallization is the predominant crystallization mechanism, $n = m = 1$ for all heating rates and Eq. (1) reduces to the well-known Kissinger equation.[32]

The Q values of glasses can be calculated by a method proposed by Ozawa[35] to deduce the order of the crystallization reaction (n) from the variation of the volume fraction (x) of crystals precipitated in a glass at a given DTA heating rate, Φ. The relation between $\ln[-\ln(1-x)]$ and $\ln x$ at constant temperature is shown by the equation below:

$$\left|\frac{\mathrm{d}(\ln(-\ln(1-x)))}{\mathrm{d}\ln\phi}\right|_T = -n \tag{2}$$

The value of n, which is an integer constant depending on the morphology of the growth when the nuclei start to form, can be evaluated by plotting $\ln[-\ln(1-x)]$ versus $\ln\Phi$ at different Φ. Here, x is obtained from the crystallization exothermic peaks at the same temperature but at different Φ.[35]

Fig. 9 a represents the respective Ozawa plots ($\ln(-\ln(1-x))$ versus $\ln\Phi$) of the exothermic peak pertaining the $0.95TeO_2$–$0.05K_2O$ sample (Fig. 8a). The Avrami parameters, n, were determined from the slope of the curve and found to be 0.88

Table 3
Values of n and m for different crystallization mechanisms during heat treatment of glass systems[33,34]

Crystallization mechanism	Kind of growth	n	m
Bulk crystallization with a constant number of nuclei (i.e. the number of nuclei is independent of the heating rate)	Three-dimensional	3	3
	Two-dimensional	2	2
	One-dimensional	1	1
Bulk crystallization with an increasing number of nuclei (i.e. the number of nuclei is inversely proportional to the heating rate)	Three-dimensional	4	3
	Two-dimensional	3	2
	One-dimensional	2	1
	Surface crystallization	1	1

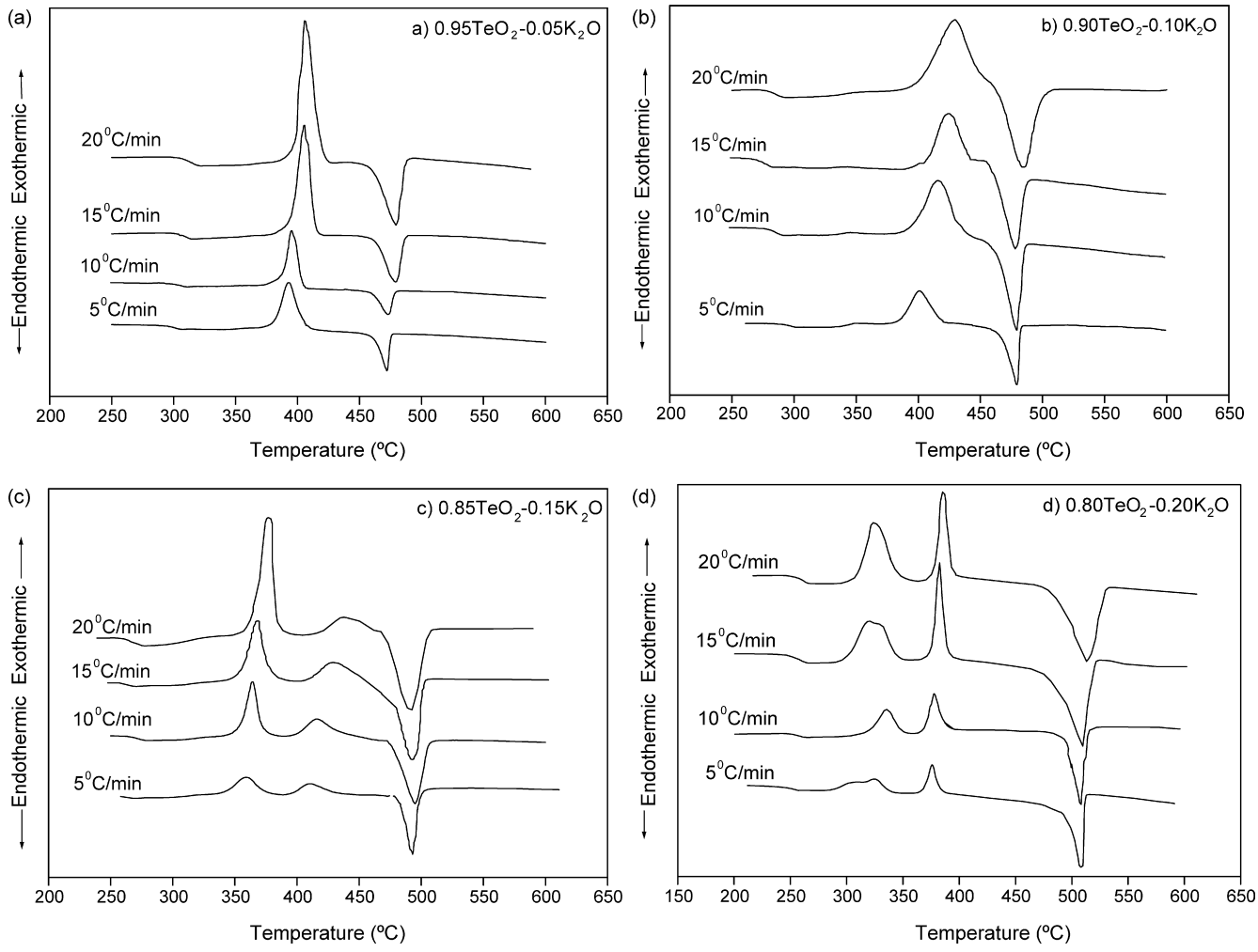

Fig. 8. DTA curves of the (a) $0.95TeO_2$–$0.05\ K_2O$, (b) $0.90TeO_2$–$0.10\ K_2O$, (c) $0.85TeO_2$–$0.15\ K_2O$, and (d) $0.80TeO_2$–$0.20K_2O$ glasses scanned at heating rates of 5, 10, 15, 20 °C/min.

and considering experimental errors, this value can be taken as $n = 1$. Thus, according to the Table 3, this result revealed that the crystalline phase occurs via surface crystallization mechanism. The activation energy of the crystallization peaks was determined by plotting $\ln(\Phi^n / T_p^2)$ versus $(1/T_p)$ given in Fig. 9b and was found to be 559.8 kJ/mol. Fig. 10 a and b shows plots of $\ln(\Phi^n / T_p^2)$ versus $(1/T_p)$ and $\ln(-\ln(1-x))$ versus $\ln \Phi$ for the $0.90TeO_2$–$0.10K_2O$ glass sample, respectively. The Avrami

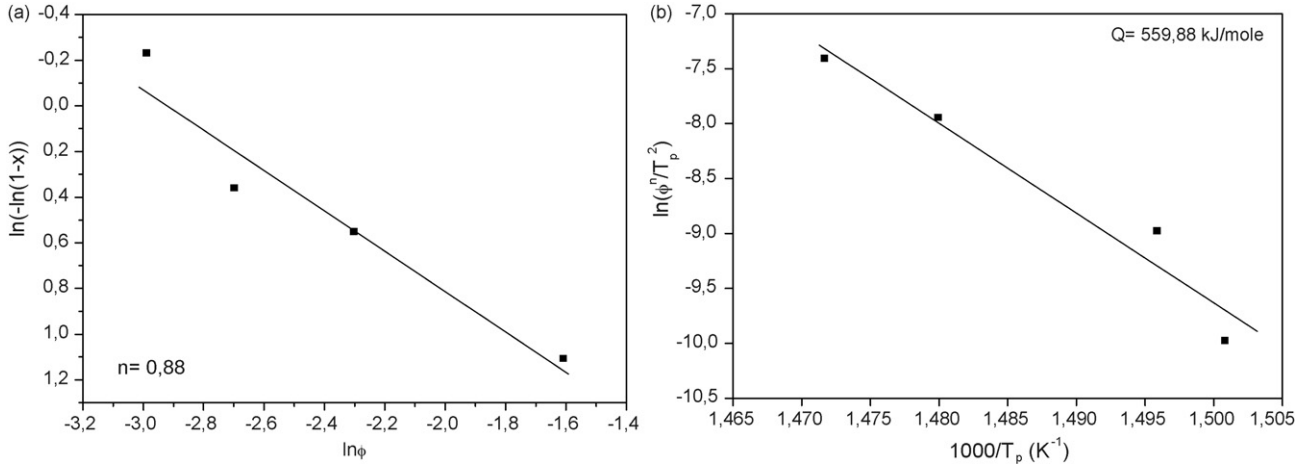

Fig. 9. (a) Ozawa plot and (b) modified Kissinger plot associated with the exotherm (T_p) of the $0.95TeO_2$–$0.05\ K_2O$ glass shown in Fig. 1.

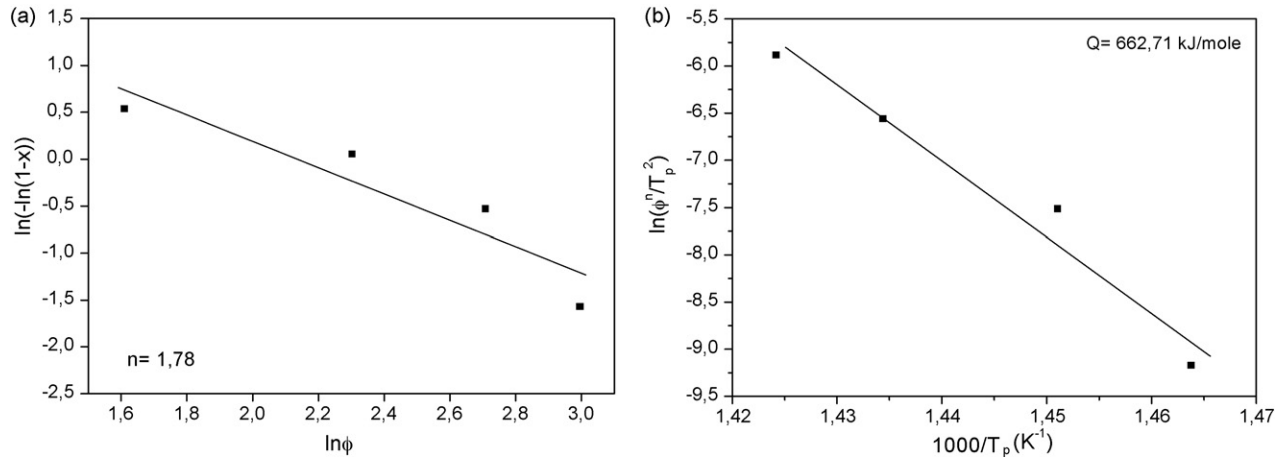

Fig. 10. (a) Ozawa plot and (b) modified Kissinger plot associated with the exotherm (T_p) of the $0.90TeO_2$–$0.10\ K_2O$ glass shown in Fig. 1.

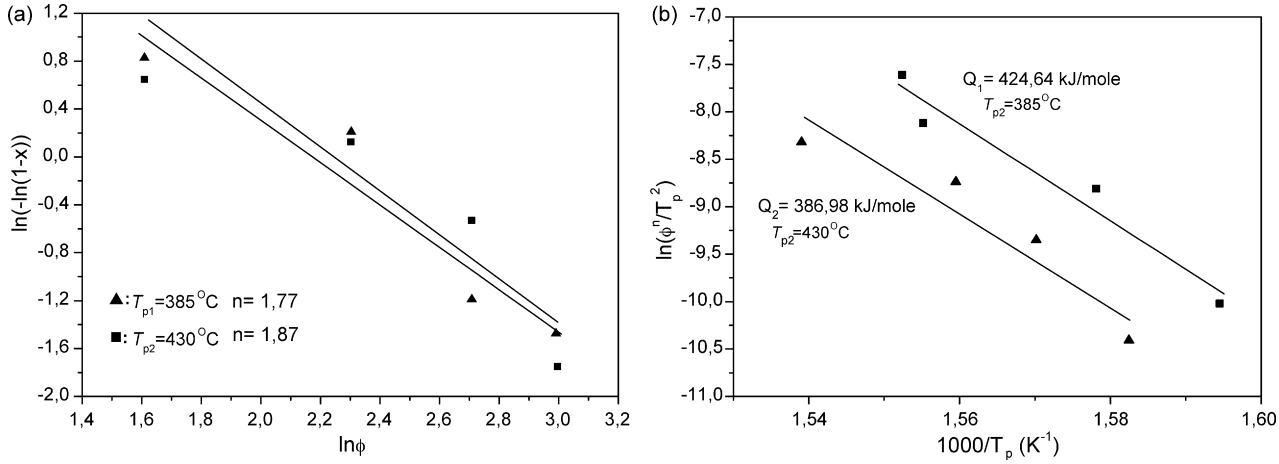

Fig. 11. (a) Ozawa and (b) modified Kissinger plots associated with the first exotherm (T_{p1}) and the second exotherm (T_{p2}) of the $0.85TeO_2$–$0.15K_2O$ glass shown in Fig. 1.

parameter n and crystallization activation energy were calculated from the volume fraction for the crystallization peak and, found to be 1.78 (Fig. 10a), and 662.7 kJ/mol (Fig. 10b), respectively. Thus, as listed in Table 3, this result corresponds to one-dimensional growth of crystals. Fig. 11a and b represent the modified Kissinger and Ozawa plots of the $0.85TeO_2$–$0.15K_2O$ sample related to the first and second exothermic peak shown in Fig. 1c. The Avrami parameters n were determined from

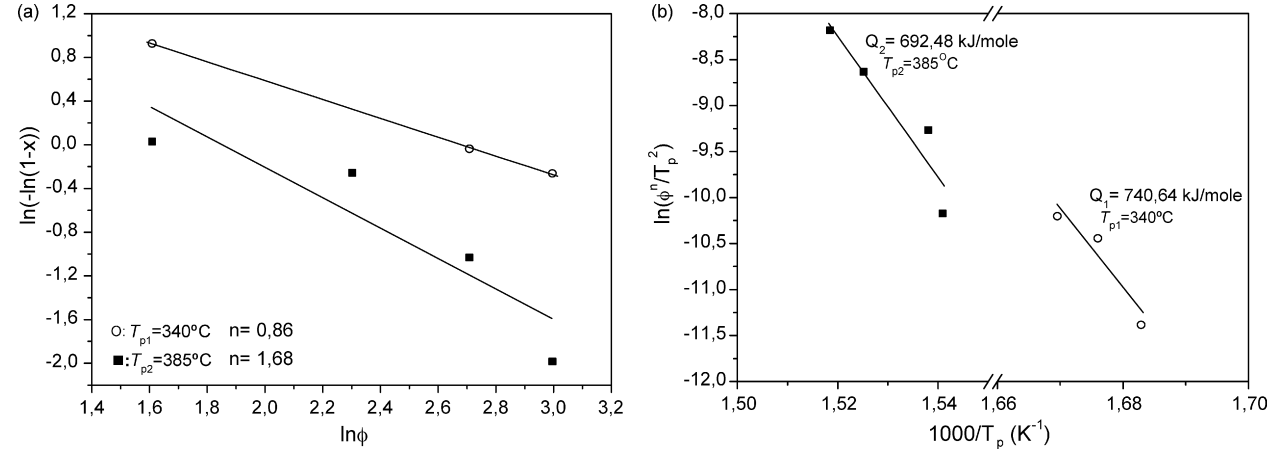

Fig. 12. (a) Ozawa and (b) modified Kissinger plots associated with the first exotherm (T_{p1}) and the second exotherm (T_{p2}) of the $0.80TeO_2$–$0.20K_2O$ glass shown in Fig. 1.

the slope of these curves and found to be 1.77 for the first exotherm and 1.87 for the second exotherm. Again, these values can be taken as $n = 2$ for both exotherms. According to Table 3, these results correspond to one-dimensional growth of crystals which is dominant for both crystallization peaks shown in Fig. 8c in this sample. The crystallization activation energies were found to be 424.6 kJ/mol for the first exotherm and 386.9 kJ/mol for the second exotherm. The DTA curves for the $0.80TeO_2$–$0.20K_2O$ sample taken at different heating rates are represented in Fig. 8. The first exothermic peak was left out of the theoretical calculations due to its paradoxical behaviour seen in Fig. 8d and only the second exothermic peak was taken into account. Fig. 12a and b is the respective modified Kissinger and Ozawa plots and 1.68 for the second peak, which means that one-dimensional crystal growth is dominant for the temperatures above the second crystallization peak in this sample. As seen in Fig. 12a, the activation energy for crystallization corresponding to the second exotherm in Fig. 8d is calculated as 692.5 kJ/mol.

4. Conclusions

Based on the results reported in the present investigation, the following conclusions can be drawn:

(1) DTA investigations have shown that increasing the K_2O content in the $(1-x)TeO_2$–xK_2O ($x = 0.05$, 0.10, 0.15, and 0.20 in molar ratio) glasses decreases the glass transition temperature, T_g. Further, the crystallization of the $(1-x)TeO_2$–xK_2O ($x = 0.05$, 0.10, 0.15, and 0.20 in molar ratio) glasses take place in the range between 327 and 421 °C with one exothermic peak for the $0.95TeO_2$–$0.05K_2O$ and $0.90TeO_2$–$0.10K_2O$ glasses and two exotherms for the $0.85TeO_2$–$0.15K_2O$ and $0.80TeO_2$–$0.20K_2O$ glasses in the DTA curves. XRD and Raman spectrophotometry investigations revealed the presence of α-TeO_2, γ-TeO_2 and $K_2Te_4O_9$ crystal phases in the $(1-x)TeO_2$–xK_2O ($x = 0.05$, 0.10, 0.15, and 0.20 in molar ratio) glass samples heated above the peak crystallization temperatures, T_p.

(2) SEM and SEM/EDS investigations of the $(1-x)TeO_2$–xK_2O ($x = 0.05$, 0.10, 0.15, and 0.20 in molar ratio) glasses heated above the peak crystallization temperatures revealed the presence of distinct TeO_2-rich and $K_2Te_4O_9$ crystals and regions comprising different mixtures of both crystals existing in the amorphous glass matrix. In the case of the $0.95TeO_2$–$0.05K_2O$ glass, the TeO_2-rich crystals were centrosymmetrically oriented long stripes and were between 20–30 μm in width and 120–220 μm in length and the $K_2Te_4O_9$ crystals were rectangular in shape and were between 2 and 5 μm in size. Both types of crystals were formed as a result of surface crystallization. On the other hand, the microstructures of the $0.90TeO_2$–$0.10K_2O$, $0.85TeO_2$–$0.15K_2O$ and $0.80TeO_2$–$0.20K_2O$ glasses comprised angular wedge-shaped regions existed both in the surface and cross-section having varying amounts of Te, O and K. Further, the $0.85TeO_2$–$0.15K_2O$ sample contained colonies of pure polygonal-shaped $K_2Te_4O_9$ crystalline phases between 4 and 20 μm in size both in the surface and cross-section.

(3) The crystallization kinetics of the $(1-x)TeO_2$–xK_2O ($x = 0.05$, 0.10, 0.15, and 0.20 in molar ratio) glasses were investigated using DTA in non-isothermal conditions. Using the Ozawa equation, the Avrami constant n was calculated as 0.94 for the $0.95TeO_2$–$0.05K_2O$ glass, indicating that surface crystallization is the dominant crystallization mechanism. Using the modified Kissinger equation, the activation energy of crystal growth for the $0.95TeO_2$–$0.05K_2O$ glass were determined as 559.9 kJ/mol. On the other hand, using the Ozawa equation, the n values were found to vary between 1.7 and 1.87 for the exothermic peaks of the $0.90TeO_2$–$0.10K_2O$, $0.85TeO_2$–$0.15K_2O$ and $0.80TeO_2$–$0.20K_2O$ glasses, indicating that one-dimensional growth of crystals ($m = 1$) is the dominant crystallization mechanism for these glasses. Activation energies for one-dimensional crystal growth mechanisms in these crystals determined from the modified Kissinger plots were found to vary between 550 and 650 kJ/mol.

Acknowledgements

The authors express their thanks to Prof. Dr. Mustafa Ürgen for the use of the X-ray diffractometer. The authors also thank Sevgin Türkeli for recording the XRD patterns and Çiğdem Çakır for her support in the SEM investigations. This research was made possible by a research grant provided by the State Planning Organization (DPT) under the Project title and number: "Advanced Technologies in Engineering—2001K 750-90146" and this is gratefully acknowledged.

References

1. El-Mallawany, R. A. H., *Tellurite Glasses Handbook: Physical Properties and Data*. CRC Press, New York, 2002.
2. Wang, J. S., Vogel, E. M. and Snitzer, E., Tellurite glasses: a new candidate for fiber devices. *Opt. Mater.*, 1994, **3**, 187–203.
3. Özen, G., Demirata, B., Öveçoğlu, M. L. and Genç, A., Thermal and optical properties of Tm^{3+} doped tellurite glasses. *Spectrochim. Acta A: Mol. Bimol. Spectrosc.*, 2001, **57**, 273–280.
4. Kim, S. H. and Yoko, T., Nonlinear optical properties of TeO_2-based glasses: MO_x–TeO_2 (M = Sc, Ti, V, Nb, Mo, Ta, and W) binary glasses. *J. Am. Ceram. Soc.*, 1995, **78**(4), 1061–1065.
5. Auzel, F., Upconversion and anti-stokes with f and d ions in solids. *Chem. Rev.*, 2004, **104**(1), 139–173.
6. Heo, J., Lam, D., Sigel Jr., G. H., Mendoza, E. A. and Hensley, D. A., Spectroscopic analysis of the structure and properties of alkali tellurite glasses. *J. Am. Ceram. Soc.*, 1992, **75**, 277–281.
7. Sidkey, M. A. and Gaafar, M. S., Ultrasonic studies on network structures of ternary TeO_2–WO_3–K_2O glass system. *Physica B*, 2004, **348**, 46–55.
8. Mochida, N., Sekiya, T. and Ohtsuka, A., Property and structure of glasses in the system TeO_2–P_2O_5. *J. Ceram. Soc. Jpn.*, 1988, **96**(10), 973–979.
9. Öveçoğlu, M. L., Özalp, M. R., Özen, G., Altın, F. and Kalem, V., Crystallization behavior of some TeO_2–ZnO glasses. *Key Eng. Mater.*, 2004, **264–268**, 1891–1894.
10. Yinnon, H., Applications of thermoanalytical techniques to the study of crystallization kinetics in glass-forming liquids. Part I. Theory. *J. Non-Cryst. Solids*, 1987, **54**, 253–275.

11. Sekiya, T., Mochida, N., Ohtsuka, A. and Mamoru, T., Raman spectra of $MO_{1/2}$–TeO_2 (M = Li, Na, K, Rb, Cs and Tl) glasses. *J. Non-Cryst. Solids*, 1992, **144**, 128–144.
12. Akagi, R., Handa, K., Ohtori, N., Hannon, A. C., Tatsumisago, M. and Umesaki, N., High-temperature structure of K_2O–TeO_2 glasses. *J. Non-Cryst. Solids*, 1999, **256–257**, 111–118.
13. El-Mallawany, R., Devitrification and vitrification of tellurite glasses. *J. Mater. Sci. Electr.*, 1995, **6**, 1–3.
14. Hart, R. T., Structures and optical properties of tellurite glass and glass ceramics. PhD Thesis. Dept. of Chemistry, Indiana University, Indiana, USA, 2004.
15. *Powder Diffraction Files: Card No. 28-806, Database Edition, Joint Committee on Powder Diffraction Standards (JCPDS)*. Stanworth, PA, USA, 1992.
16. Tagg, S. L., Structural investigations of alkali tellurite crystals and glasses utilizing diffraction and spectroscopic techniques. PhD Thesis. Dept. of Chemistry, Indiana University, Indiana, USA, 1997.
17. Öz, B., Kabalcı, İ., Öveçoğlu, M. L. and Özen, G., Thermal properties and crystallization Behavior of some TeO_2–K_2O glasses. *J. Eur. Ceram. Soc.*, 2007, **27**, 1823–1827.
18. *Powder Diffraction Files: Card No. 42-1365, Database Edition, Joint Committee on Powder Diffraction Standards (JCPDS)*. Stanworth, PA, USA, 1992.
19. *Powder Diffraction Files: Card No. 9-433, Database Edition, Joint Committee on Powder Diffraction Standards (JCPDS)*. Stanworth, PA, USA, 1992.
20. Blanchandin, S., Marchet, P., Thomas, P., Champarnaud-Mesjard, J. C., Frit, B. and Chagraoui, A., New Investigations within the TeO_2–WO_3 system. *J. Mater. Sci.*, 1999, **34**(17), 4285–4292.
21. Öveçoğlu, M. L., Özen, G. and Cenk, S., Microstructural characterization and crystallization behavior of $(1-x)TeO_2$–xWO_3 ($x = 0.15, 0.25, 0.3$ mol) glasses. *J. Eur. Ceram. Soc.*, 2006, **26**(7), 1149–1158.
22. Wang, G., Zhang, J., Dai, S., Yang, J. and Jiang, Z., Thermal analyses, spectral characterization and structural interpretation of Yb^{3+} doped TeO_2–ZnO–$ZnCl_2$ glasses. *Phys. Lett. A*, 2005, **341**, 285–290.
23. Pan, Z. and Morgan, S., Raman spectra and thermal analysis of a new lead–tellurium–germanate glass system. *J. Non-Cryst. Solids*, 1997, **210**, 130–135.
24. Wang, G., Zhang, J., Dai, S., Wen, L., Yang, J. and Jiang, Z., Structural investigation on TeO_2–$BiCl_3$ glassy system. *J. Mol. Struct.*, 2005, **750**(1–3), 1–6.
25. Mattarelli, M., Chiappini, A., Montagna, M., Martucci, A., Ribaudo, A., Guglielmi, M. *et al.*, Optical spectroscopy of TeO_2–GeO_2 glasses activated with Er^{3+} and Tm^{3+} ions. *J. Non-Cryst. Solids*, 2005, **351**, 1759–1763.
26. Kosuge, T., Benino, Y., Dimitrov, V., Sato, R. and Komatsu, T., *J. Non-Cryst. Solids*, 1998, **242**, 154–164.
27. Mirgorodsky, A. P., Merle-Me'jean, T., Champarnaud, J.-C., Thomas, P. and Frit, B., Dynamics and structure of TeO_2 polymorphs: model treatment of paratellurite and tellurite; Raman scattering evidence for new γ- and δ-phases. *J. Phys. Chem. Solids*, 2000, **61**, 501–509.
28. Chowdari, B. V. R. and Kumari, P. P., Structure and ionic conduction in the $Ag_2O{\cdot}WO_3{\cdot}TeO_2$ glass system. *J. Mater. Sci.*, 1998, **33**, 3591–3599.
29. Charton, P., Thomas, P. and Armand, P., Raman and crystallization behaviours of TeO_2–Sb_2O_5 glasses. *J. Non-Cryst. Solids*, 2003, **321**, 81–88.
30. Ray, C. S., Yang, Q., Huang, W. and Day, D. E., Surface and internal crystallization in glasses as determined by differential thermal analysis. *J. Am. Ceram. Soc.*, 1996, **79**(12), 155–3160.
31. Erol, M., Küçükbayrak, S., Ersoy-Meriçboyu, A. and Öveçoğlu, M. L., Crystallization behaviour of glasses produced from fly ash. *J. Eur. Ceram. Soc.*, 2001, **21**, 2835–2841.
32. Kissinger, H. E., Variation of peak temperature with heating rate in differential thermal analysis. *J. Res. Nat. Bur. Stand.*, 1956, **57**, 217–221.
33. Matusita, K., Sakka, S. and Matsui, Y., Determination of the activation energy for crystal growth by DTA. *J. Mater. Sci.*, 1975, **10**, 961–966.
34. Matusita, K. and Sakka, S., Kinetic study on crystallization of the glass by DTA-criterion on application of Kissinger plot. *J. Non-Cryst. Solids*, 1980, **38–39**, 741–746.
35. Ozawa, T., Kinetics of non-isothermal crystallization. *Polymer*, 1971, **12**, 150–158.